GEOPHYSICS, VOL. 65, NO. 2 (MARCH-APRIL 2000); P. 521–525, 8 FIGS., 2 TABLES.

Short Note

GPR modeling study in a contaminated area of Krzywa Air Base (Poland)

José M. Carcione*, Henryk Marcak‡, Géza Seriani*, and Giorgio Padoan*

INTRODUCTION

Krzywa Air Base is a former Soviet military base which is highly polluted because of soil contamination during the dismantling of fuel tanks after the 1990 political changes in the U.S.S.R. The contaminated sites are indicated as magazines 1 and 2 in Figure 1. The area is located within the pre-Sudetic block, where Tertiary and Quaternary deposits lie on Mesozoic crystalline basement. The deposits consist of sands of different grain sizes, gravels, clays, and interbedded silts, with a total thickness ranging from 80 to 100 m. In the extreme cases, the pollution is so intense that the spilled fuel can be extracted in the system of drainage wells. In general, the contamination can be correlated with the geologic structure. As a prelude to acquisition of field data, we simulate and evaluate the expected ground-penetrating radar (GPR) responses for uncontaminated and contaminated layers.

Using these calibrations, the geometric features of hydrocarbon-contaminated zones lying on the water table can be identified and mapped in simulated GPR data. Because aviation gasoline has a relative dielectric constant of 2 and water has a relative dielectric constant of 80, the detection is based mainly on the permittivity contrast between the hydrocarbon and groundwater-saturated layers. Differences in conductivity (10^{-3} S/m for rainwater versus 10^{-6} S/m for gasoline) provide an additional constraint to aid in the interpretation of the radargrams.

A typical hydrocarbon spill in the subsurface consists of various components. A capillary fringe and a gaseous zone develop above the water table, and the product core is, in general, located above the water table, with a diffuse mixing region below. Hydrocarbons do not disperse in a homogeneous way because they form a partially dissolved phase mixed with air (gas) and water, as a consequence of rainfall, seasonal variations, and the hydrogeologic conditions in the area. Here, we simplify the problem by assuming a sharp interface between the contaminated and uncontaminated regions, i.e., neglecting capillary effects. Subject to this assumption, we evaluate the minimal degree of hydrocarbon saturation that can be detected with the GPR technique and, in addition, determine the antenna frequency required to resolve the contaminated layer.

The radar simulation is based on the forward-modeling code developed by Carcione (1996). The model for computing the effective permittivities and conductivities of sand/clay mixtures is given in Carcione and Seriani (2000). This model, based on a self-similar theory for the sandy component and a transversely isotropic constitutive equation for the shaly component, gives the soil electromagnetic properties as a function of clay content and pore fluid saturations. The results of the survey simulation may be field tested by acquisition of real data in the future.

MODEL AND ELECTROMAGNETIC PROPERTIES

The model (Figure 2) is a vertical section around well 39/1 in magazine 1 (Figure 1). It was interpreted from the stratigraphic columns of wells 39/1 and VII/1, and it includes a contaminated region indicated by the gray color (Figure 2). The soil model is parameterized in terms of a porosity ϕ; a sand proportion ϕ_q; a clay/silt proportion ϕ_{cs}; and water, air, and hydrocarbon saturations denoted by S_w, S_a, and S_c, respectively. Table 1 gives the properties of the individual constituents at 200 MHz. The dielectric properties of water and clay are described by a Cole-Cole model, which simulates the dissipation and dispersion effects caused by the relaxation of the water molecule (with a relaxation peak at 10 GHz) (Carcione and Seriani, 2000).

Table 2 contains the effective electromagnetic properties of the different soils composing the geologic cross-section, calculated with the model developed by Carcione and Seriani

Manuscript received by the Editor September 29, 1998; revised manuscript received July 16, 1999.
*Osservatorio Geofisico Sperimentale, Borgo Grotta Gigante 42c, 34010 Sgonico, Trieste, Italy. E-mail: jcarcione@ogs.trieste.it. E-mail: gseriani@ogs.trieste.it; gpadoan@ogs.trieste.it.
‡Institute of Geophysics, University of Mining and Metallurgy, Al. Mickiewicza 30, 30-059 Kraków, Poland. E-mail: marcak@uci.agh.edu.pl.

(2000). The main differences among gravel, fine-grain sand, and medium-grain sand are caused by porosity. The packing of sand grains depends on the size of the asperities, which are larger for gravel than for fine- and medium-grain sands. The presence of clay induces anisotropy, i.e., the larger the clay content, the larger the degree of anisotropy. Pure sands, with no clay content, are assumed to be isotropic. The effective permittivity is fairly constant in the radar frequency range, and the effective conductivity is higher at 200 MHz because of dissipation caused by the water-relaxation phenomenon.

Figure 3 illustrates the effective dielectric constant for sand partially saturated with aviation gasoline, water, and air (Carcione and Seriani, 2000). The continuous lines correspond to constant water saturation (no italics) and the broken lines to constant air saturation (italics). The dielectric properties of water-saturated sand, indicated in Table 2, can be obtained from Figure 3. The soil fully saturated with water has a permittivity of 21.6 ϵ_0. For instance, if $S_c = 0.4$ and $S_w = 0.4$, $S_a = 1.0 - S_w - S_c = 0.2$, the effective permittivity will be equal to 9 ϵ_0; full air saturation corresponds to $S_w = S_c = 0$, with a permittivity of $3\epsilon_0$ (the lower value of the curve $S_w = 0$); full gasoline saturation, i.e., $S_c = 1$, implies a permittivity of nearly 3.5 ϵ_0 (the highest value of the curve $S_w = 0$). For a given water saturation, the dielectric constant increases with increasing hydrocarbon saturation because aviation gasoline has higher permittivity than air. For a given air saturation, the effective permittivity increases with increasing water saturation because water has a much higher permittivity than aviation gasoline.

THE RADARGRAMS

The geologic model has a horizontal extent of 15 m, with well 39/1 at its center. The numerical mesh has $N_X = 243$ and $N_Z = 243$ grid points, with a grid spacing $D_X = D_Z = 7.5$ cm. The source is a Ricker-type wavelet applied as a vertically propagating "plane wave" to approximate (very roughly but efficiently) a stacked seismogram (Carcione et al., 1994). The

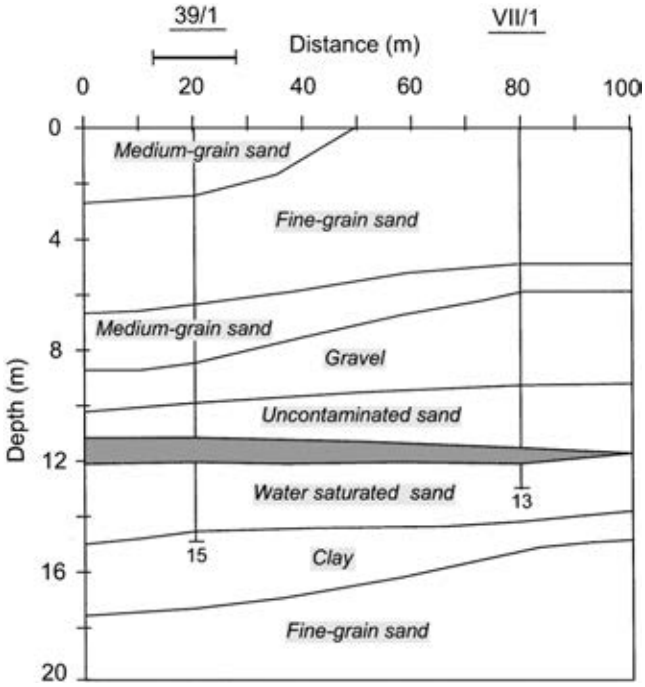

FIG. 2. A segment of the interpreted geologic section containing wells 39/1 and VII/1. The contaminated region is shown in gray. The portion used in radar modeling is shown by a bar (top).

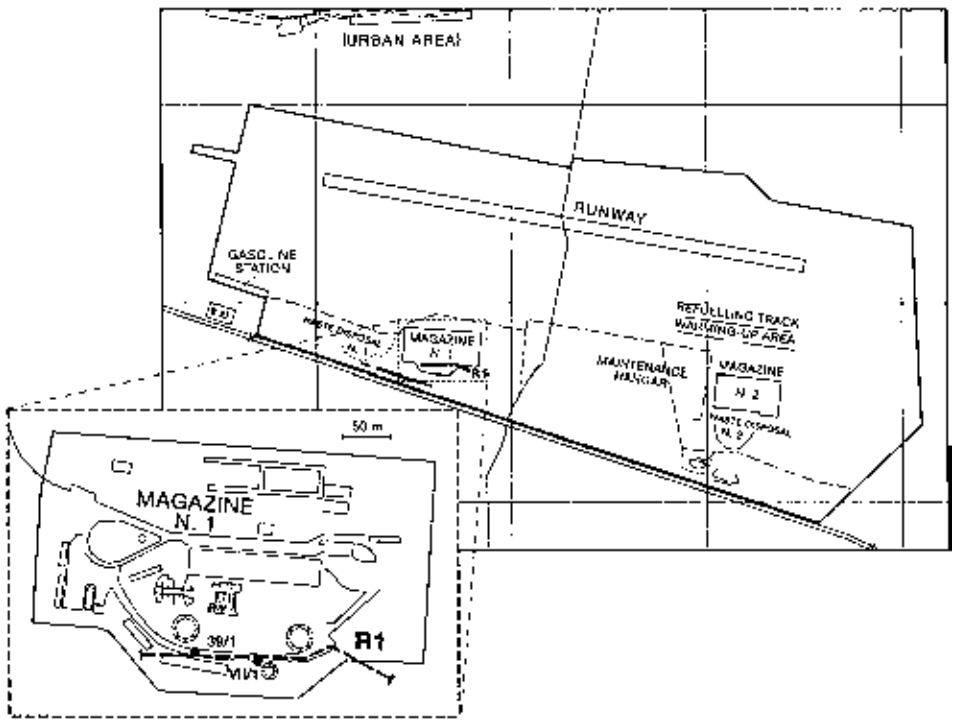

FIG. 1. Map of Krzywa Air Base and details of magazine 1 with the location of wells 39/1 and VII/1.

source is polarized in the horizontal direction. The 2-D numerical modeling algorithm is similar to that used in Carcione (1996) and uses a time step of 0.05 ns. Figure 4 shows the synthetic radargrams of the horizontal (transverse) electric field for a 200-MHz antenna and a hydrocarbon saturation of 30%. The synthetic radargrams for a 50-MHz antenna are represented in Figure 5, where the top figure (a) corresponds to the uncontaminated case and the bottom figure (b) to a hydrocarbon saturation of 30%. The mark indicates the reflection corresponding to the top of the contaminated layer, which has a thickness of approximately 75 cm. The top and bottom of this layer can be seen clearly in the 200-MHz radargram, and 50 MHz is close to the resolution limit. However, the reflection from the bottom is stronger for the 30% contaminated layer than for the uncontaminated layer, since the radar has less attenuation because of the lower conductivity of the soil (Table 2). The radargram for 10% contamination, obtained with the 50-MHz antenna, is shown in Figure 6. The top reflection barely can be seen in this case.

The "visibility" of the reflection from the top of the contaminated layer depends in part on the radar performance Q (the ratio of the transmitter signal [energy] to the minimum receiver sensitivity). In the past, GPR systems have had performances of 80-120 dB, whereas the newer radars have system performances of 120-160 dB (see Davis and Annan, 1989, for further details). Figure 7 shows the 200-MHz normalized radar traces (at 7-m horizontal position) between 200 and 250 ns, for 0%, 10%, and 30% contamination. The mark indicates the reflection from the top of the contaminated region. Note that for 30% contamination, the event corresponding to the bottom of the layer (the stronger pulse) precedes the reflection corresponding to the uncontaminated case. This effect is caused by the lower permittivity of gasoline with respect to water, implying higher-phase velocities. It can be shown that the effects of velocity dispersion are negligible in the sands overlying the contaminated layer. Assume a radar performance of 140 dB, such that the dynamic range for amplitudes is 70 dB. Recall that $x(\text{dB})$ equals $10\log_{10}(A_1^2/A_2^2)$ for energy and $20\log_{10}(A_1/A_2)$ for amplitudes, where A_1 is the input amplitude and A_2 is the amplitude of the reflected pulse. For the traces represented in Figure 7, the ratio of input amplitude to reflection amplitude is 20 dB for 30% contamination and 30 dB for 10% contamination. To exceed 70 dB, the simulations indicate that the saturation should be lower than 0.1%. A rough estimation of this value also can be obtained from the normal-incidence reflection coefficient versus gasoline saturation, assuming that the Q ratio (in dB) is proportional to the logarithm of the reflection coefficient (Davis and Annan, 1989). For lossy media, the normal-incidence reflection coefficient, for a reflection from layer $l = 2$ incident to layer $l = 1$, can be expressed as

$$R = \frac{\sqrt{\epsilon_1^*} - \sqrt{\epsilon_2^*}}{\sqrt{\epsilon_1^*} + \sqrt{\epsilon_2^*}}, \quad \epsilon_\ell^* = \epsilon_\ell - \frac{i}{\omega}\sigma_\ell, \quad \ell = 1, 2, \qquad (1)$$

where ω is the angular frequency and ϵ_ℓ and σ_ℓ are given in Table 2. The absolute value of R from the top of the layer versus gasoline saturation is shown in Figure 8. A linear relation between Q and $\log_{10}(|R|)$, based on the dB values for 10% and 30% saturation, gives 50 dB for 1% saturation and 70 dB for 0.1% saturation, in agreement with the simulations.

Table 1. Electromagnetic properties*.

Medium	ϵ (ϵ_0)	σ (S/m)
Quartz**	4.5	10^{-6}
Clay/silt	20	0.1
Air** (gas)	1	0
Rainwater**	80.1	0.001
Aviation gasoline†	2	10^{-6}

*$\epsilon_0 = 8.85\ 10^{-12}$ F/m; $\mu_0 = 4\pi\ 10^{-7}$ H/m.
**Schön (1996).
†Von Hippel (1961).

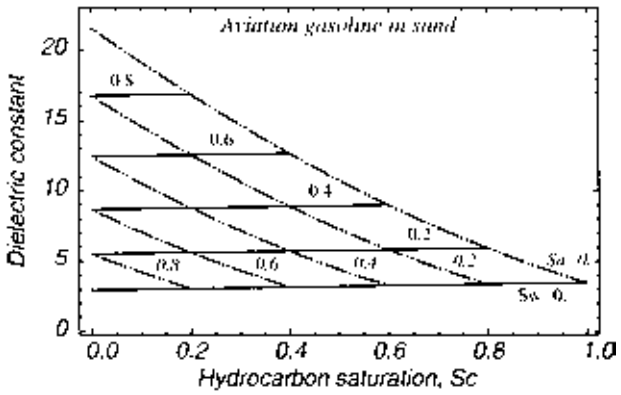

FIG. 3. Effective dielectric constant for sand partially saturated with aviation gasoline, water, and air, versus gasoline saturation. The continuous lines correspond to constant water saturation, S_w (no italics), and the broken lines correspond to constant air saturation, S_a (italics).

Table 2. Soil electromagnetic properties.

							50 MHz		200 MHz	
Medium	ϕ_q	ϕ_{cs}	ϕ	S_w	S_a	S_c	ϵ (ϵ_0)	σ (mS/m)	ϵ (ϵ_0)	σ (mS/m)
Medium-grain sand	0.65	0	0.35	0.2	0.8	0	5.5	0.04	5.5	0.3
Fine-grain sand	0.7	0	0.3	0.4	0.6	0	7.9	0.08	7.9	0.5
Gravel	0.6	0	0.4	0.3	0.7	0	7.5	0.08	7.5	0.5
Uncontaminated sand	0.7	0	0.3	0.6	0.4	0	11	0.14	11	0.9
Contaminated sand (1)	0.7	0	0.3	0.3	0.4	0.3	6.7	0.05	6.7	0.4
Contaminated sand (2)	0.7	0	0.3	0.5	0.4	0.1	9.4	0.1	9.4	0.7
Water-saturated sand	0.65	0	0.35	1	0	0	21.6	0.3	21.6	2.4
Clay (in bedding plane)	0	0.8	0.2	0.8	0.2	0	27.4	72.3	28.8	75.8
Clay (normal to b.p.)	0	0.8	0.2	0.8	0.2	0	18.7	18.8	13.7	31.2

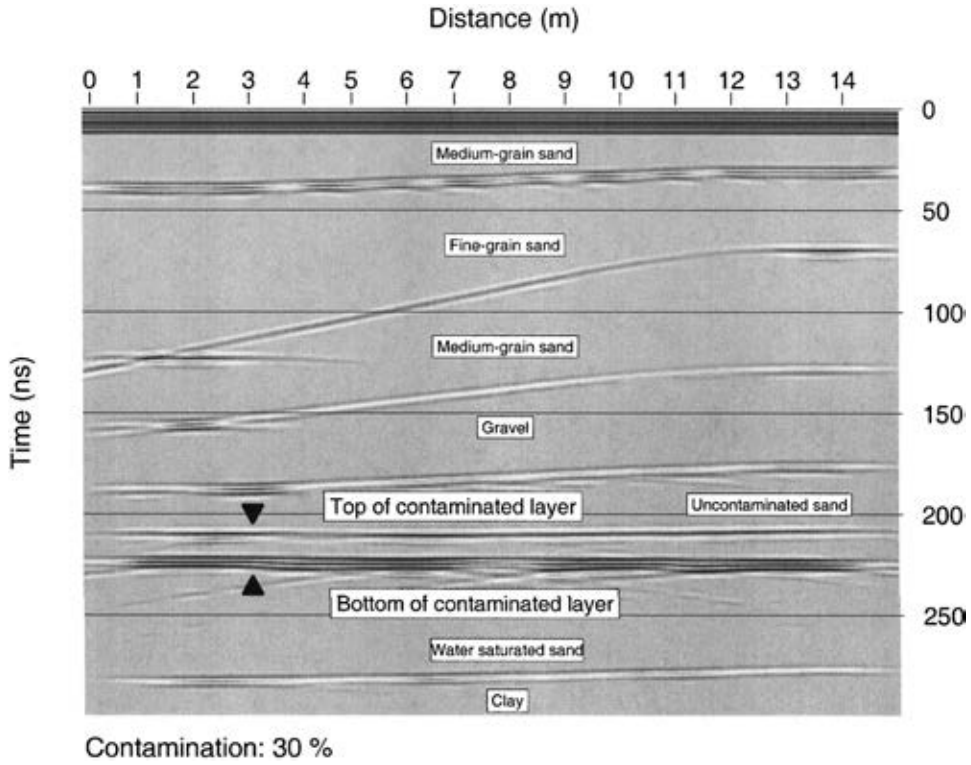

FIG. 4. Synthetic radargram of the horizontal electric field for a 200-MHz antenna, corresponding to a hydrocarbon saturation of 30%. Marks indicate the top and bottom of the contaminated region.

However, this is an ideal situation because the electromagnetic "visibility" of the contaminated region depends on other factors, such as the coverage used to acquire and process the data, the signal-to-noise ratio, the antenna separation, and the electrical properties of the overburden above the target. For instance, increasing the conductivity of the overburden by one order of magnitude (e.g., by increasing the salt content in the pore water) implies a ratio of input amplitude to reflection amplitude of 68 dB for 200 MHz and 30% contamination, which is very close to the radar performance limit.

CONCLUSIONS

The range and resolution of GPR have been quantified by simulated 2-D surveys for a contaminated area at Krzywa Air Base (Poland). Assuming that fresh water (rainwater) fills the pores of the overlying layers, the average conductivity is approximately 0.5 mS/m at 200 MHz. In this case, the top of the contaminated layer is electromagnetically visible for gasoline saturations higher than 0.1%, assuming a radar performance of 140 dB. Increasing that conductivity by an order of magnitude (i.e., to 5 mS/m) implies that saturations below 30% cannot be detected with the GPR technique. This threshold can be lowered by using lower frequencies, which have higher penetration (for a 50-MHz antenna, the average conductivity is 0.08 mS/m for fresh water filling the pores). However, 50 MHz is close to the resolution limit for layer thicknesses less than 1 m. The study indicates that the location of the contaminated layer can be detected with 200-MHz data, provided that the saturation is relatively high. Then 50-MHz data can be used to map the extent of the polluted area. Field surveys are needed to test the prediction of the simulations.

ACKNOWLEDGMENTS

This work was financed in part by the European Union under the INCO-COPERNICUS project Detection of Hydrocarbon Contaminated Soils by Electromagnetic Techniques, Contract Nr. ERBIC15CT960801.

REFERENCES

Carcione, J. M., 1996, Ground penetrating radar: wave theory and numerical simulation in lossy anisotropic media: Geophysics, **61**, 1664–1677.
Carcione, J. M., Böhm, G., and Marchetti, A., 1994, Simulation of a CMP seismic section: J. Seis. Expl., **3**, 381–396.
Carcione, J. M., and Seriani, G., 2000, An electromagnetic modelling tool for the detection of hydrocarbons in the subsoil: Geophys. Prosp., **48**.
Davis, J. L., and Annan, A. P., 1989, Ground-penetrating radar for high-resolution mapping of soil and rock stratigraphy: Geophys. Prosp., **37**, 531–551.
Schön, J. H., 1996, Physical properties of rocks: Pergamon.
Von Hippel, A. R., 1961, Dielectric materials and applications: M.I.T. Press.

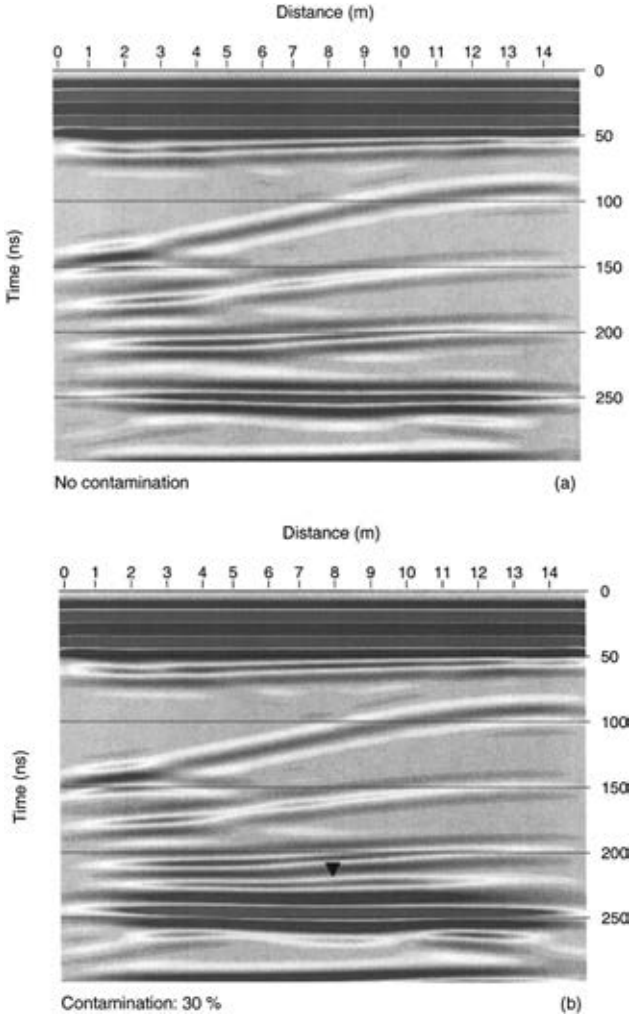

FIG. 5. Synthetic radargrams of the horizontal electric field for a 50-MHz antenna, where (a) corresponds to the model with an uncontaminated layer and (b) to a model with hydrocarbon saturation of 30%. The mark indicates the reflection from the top of the contaminated region.

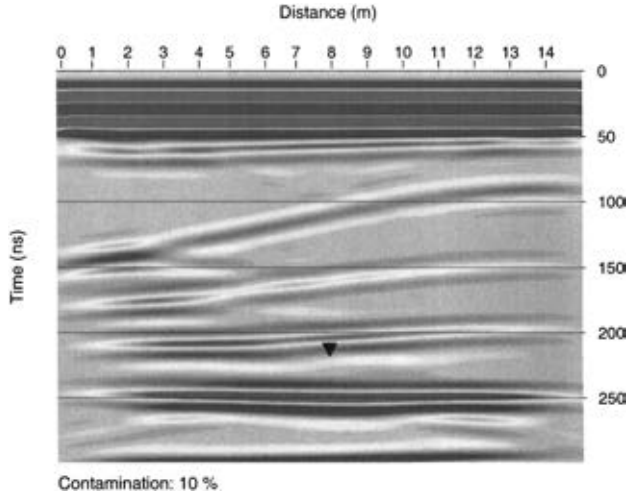

FIG. 6. Synthetic radargram of the horizontal electric field for a 50-MHz antenna, corresponding to a hydrocarbon saturation of 10%. The mark indicates the reflection from the top of the contaminated region.

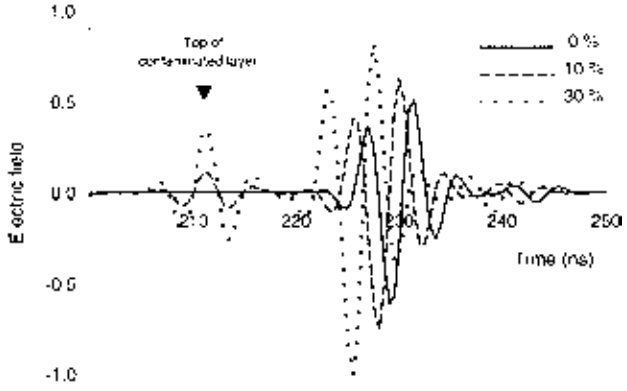

FIG. 7. Normalized radar traces (at 7-m horizontal distance) between 200 and 250 ns, for 0%, 10%, and 30% contamination. The mark indicates the top of the contaminated region.

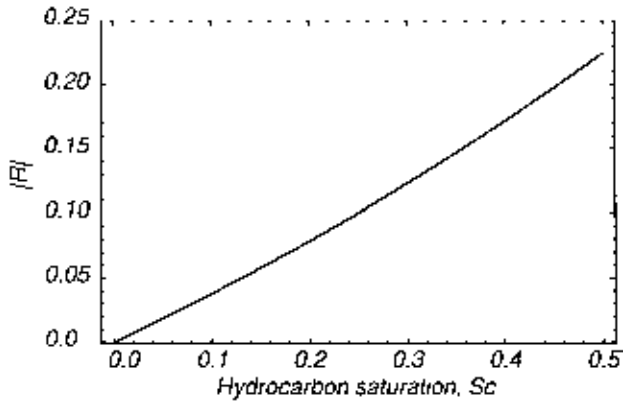

FIG. 8. Absolute value of the normal-incidence reflection coefficient versus gasoline saturation, corresponding to the top of the contaminated layer, and a frequency of 200 MHz.